

© 2019 IEEE. Personal use of this material is permitted. Permission from IEEE must be obtained for all other uses, in any current or future media, including reprinting/republishing this material for advertising or promotional purposes, creating new collective works, for resale or redistribution to servers or lists, or reuse of any copyrighted component of this work in other works.

Field Dependent Conductivity and Threshold Switching in Amorphous Chalcogenides – Modeling and Simulations of Ovonic Threshold Switches and Phase Change Memory Devices

Jake Scoggin, Helena Silva, *Senior Member, IEEE*, and Ali Gokirmak, *Senior Member, IEEE*

Abstract – We model electrical conductivity in metastable amorphous $\text{Ge}_2\text{Sb}_2\text{Te}_5$ using independent contributions from temperature and electric field to simulate phase change memory devices and Ovonic threshold switches. 3D, 2D-rotational, and 2D finite element simulations of pillar cells capture threshold switching and show filamentary conduction in the on-state. The model can be tuned to capture switching fields from ~ 5 to 40 MV/m at room temperature using the temperature dependent electrical conductivity measured for metastable amorphous GST; lower and higher fields are obtainable using different temperature dependent electrical conductivities. We use a 2D fixed out-of-plane-depth simulation to simulate an Ovonic threshold switch in series with a $\text{Ge}_2\text{Sb}_2\text{Te}_5$ phase change memory cell to emulate a crossbar memory element. The simulation reproduces the pre-switching current and voltage characteristics found experimentally for the switch + memory cell, isolated switch, and isolated memory cell.

Index Terms—Phase change memory, amorphous semiconductors, finite element analysis

I. INTRODUCTION

PHASE change memory (PCM) is a non-volatile memory that stores information as the conductive crystalline or resistive amorphous phase of a material. The crystalline-to-amorphous phase transition is controllable and reversible, with PCM attaining 10^3 x faster write times and 10^4 x better endurance than flash memory [2]. PCM is CMOS back-end-of-line compatible, allowing memory integration on-chip with CMOS circuitry to eliminate latency from off-chip memory access [3]. PCM can be implemented as a crossbar array, allowing high device density ($4F^2$) in multiple memory layers and efficient neuromorphic computing [4]. Crossbars consist of perpendicular word and bit lines with memory elements sandwiched between these lines at the cross-points (Fig. 1). Each word or bit line is connected to V_{dd} or ground through a transistor, and cross-points can be randomly accessed by activating their corresponding word and bit lines. Non-selected

devices can form undesirable current sneak paths between selected and non-selected lines; hence access devices with non-linear current-voltage (I - V) characteristics, high I_{on}/I_{off} ratios ($I_{on}/I_{off} \sim 10^6$ for a 1000×1000 device array), and high drive capabilities to write ($I_{write} \sim \text{MA}/\text{cm}^2$) are needed at each cross-point [5]. Ovonic threshold switches (OTS) made from amorphous chalcogenides are one such access device.

Amorphous chalcogenides are highly resistive under low electric fields and exhibit “threshold switching” to a highly conductive on-state at a threshold voltage (V_{th}). Once switched, these materials remain in the on-state while a minimum holding current or voltage (I_{hold} or V_{hold}) is maintained (Fig. 2) [6].

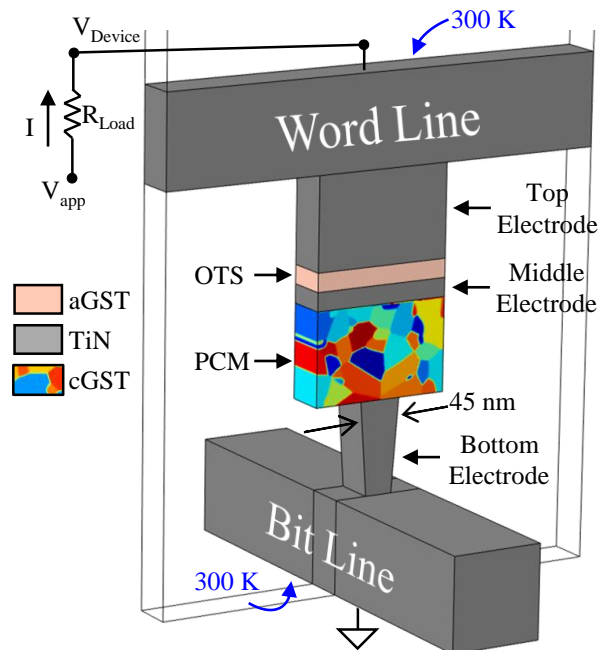


Fig. 1: A schematic illustration of a cross-point cell with an Ovonic threshold switch in series with a phase change memory element. The shown cell structure is used for 2D analysis to compare modeling results to the experimental results in [1].

Submitted on XX/XX/XXXX. This work was supported by AFOSR MURI under Award No. FA9550-14-1-0351.

The authors are with the Department of Electrical and Computer Engineering, University of Connecticut, Storrs, CT 06269 USA (email:

jacob.scoggin@uconn.edu;
ali.gokirmak@uconn.edu).

helena.silva@uconn.edu;

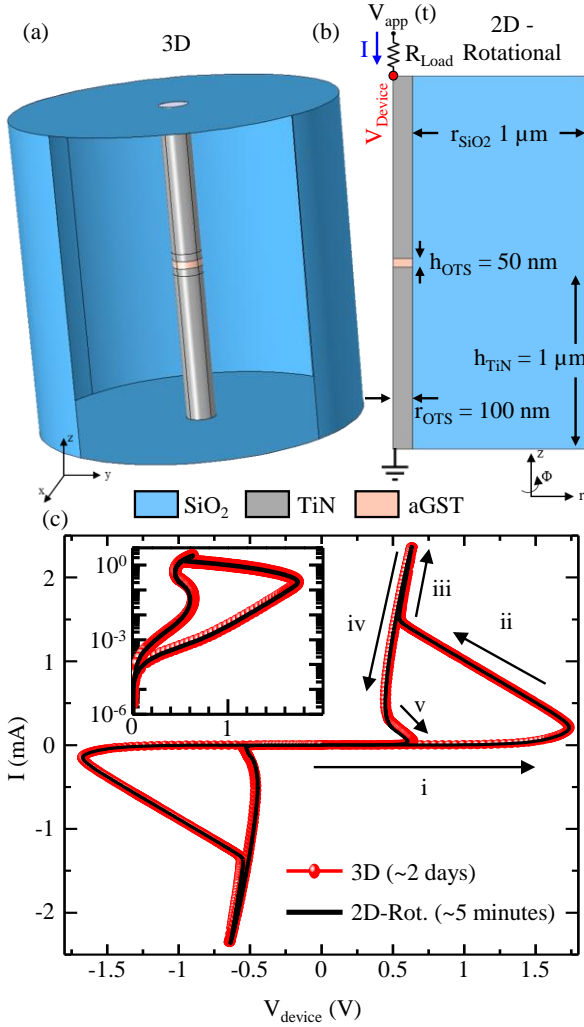


Fig. 2: (a) 3D and (b) 2D-rotational OTS geometries used in this work. $T = 300 \text{ K}$ is used as the initial condition and as the boundary condition at the top and bottom of the TiN contacts. (c) When a $3 \text{ V} / 60 \text{ ns}$ triangular pulse is applied at V_{app} , the device (i) is highly resistive until $V_{\text{switch}} \sim 1.75 \text{ V}$, (ii) switches on in $\sim 10 \text{ ps}$, (iii - iv) remains on until the voltage and current drop below $V_{\text{hold}} \sim 0.4 \text{ V}$ and $I_{\text{hold}} \sim 0.25 \text{ mA}$, and (v) returns to the high resistance off-state. Symmetric switching behavior is observed when a negative ramped pulse is applied. The 2D-rotational and 3D simulations give similar results, as expected for rotationally symmetric filamentary switching. Inset in (c) is the first quadrant in logarithmic scale.

Crystallization dynamics of these materials determine whether they are more suitable for an OTS or a PCM. PCM materials include various stoichiometries of Ag-In-Sb-Te and Ge-Sb-Te, with typical crystallization times on the order of 10 ns [7]. OTS materials remain in their amorphous phase during normal operation and are often characterized by the number of switching cycles they withstand before failure (through, e.g., material damage or crystallization): > 600 for GeTe_6 [8], $> 10^8$ for AsTeGeSiN [9], and unknown for As-doped Se-Ge-Si, a material used in a commercial OTS+PCM crossbar array [10].

There is still debate on the mechanism(s) underlying threshold switching despite many studies investigating this phenomenon [1], [6], [19], [11]–[18]. V_{th} scales linearly with

device thickness, suggesting a field-based mechanism at a threshold E_{th} [15]. Theoretical arguments and the presence of crystalline filaments in failed devices suggest that on-state conduction is filamentary [12], [15].

Current-field ($I-\vec{E}$) measurements on amorphous chalcogenides typically show an ohmic regime at low \vec{E} , an intermediate regime where $\ln(I) \propto \vec{E}$ or $\vec{E}^{\frac{1}{2}}$, and a high field regime where I increases at a super-exponential rate with \vec{E} [20]. Reference [20] reviews conduction mechanisms in amorphous materials and shows that multiple mechanisms can fit measured data through the tuning of parameters which are otherwise difficult to validate (e.g. trap-to-trap distance, effective carrier mass, and carrier mobility). Models for these mechanisms have been proposed which define carrier concentrations (n) and mobilities (μ) as functions of \vec{E} and temperature (T) such that all three $I-\vec{E}$ regimes are captured with an electrical conductivity $\sigma = qn\mu$, but such techniques are computationally expensive in addition to relying on multiple unknown fitting parameters. Reference [13] proposes a field-based switching model where carrier concentrations rapidly increase once trap states near the Fermi band are filled and fits the model to amorphous (a-) $\text{Ge}_2\text{Sb}_2\text{Te}_5$ (GST) measurements. References [18], [19] propose a field-assisted thermal model based on multiple trap barrier lowering and fit the model to a-GeTe and doped a-GST measurements. References [14], [21] ascribe switching to crystalline filaments which form under high \vec{E} and fit the model to a-GST using relaxation oscillations. They suggest that these filaments become unstable at low \vec{E} in OTS materials but remain stable in PCM materials.

Here, we model conductivity in a-GST as the sum of T and \vec{E} dependent terms ($\sigma_a = \sigma_T + \sigma_E$). This model does not require a computationally expensive evaluation of the (density of states \times Fermi function) integral at every T, \vec{E} combination where conductivity is needed; hence, it is appropriate for transient finite element simulations with dynamic T and \vec{E} . While this model trades accuracy for ease of computation, simulations show that it (i) can be tuned to fit a wide range of switching fields, (ii) captures the appropriate changes in threshold switching as we systematically vary ambient conditions, geometries, and the rise and fall times of applied pulses, and (iii) can reproduce the behavior of a series PCM+OTS device when used with a finite element phase change model [22]–[25].

II. COMPUTATIONAL MODEL

We use a-GST material parameters as in [23], [25] to simulate an OTS material. Of particular interest to this work is σ_a , which we model as in [26] and cap at $\sigma_{\text{max}} = \sigma_T(930 \text{ K})$ (Fig. 3):

$$\sigma_a(T, \vec{E}) = \min(\sigma_T(T) + \sigma_E(\vec{E}), \sigma_{\text{max}}), \quad (1)$$

which is equivalent to assuming that free carriers are excited to

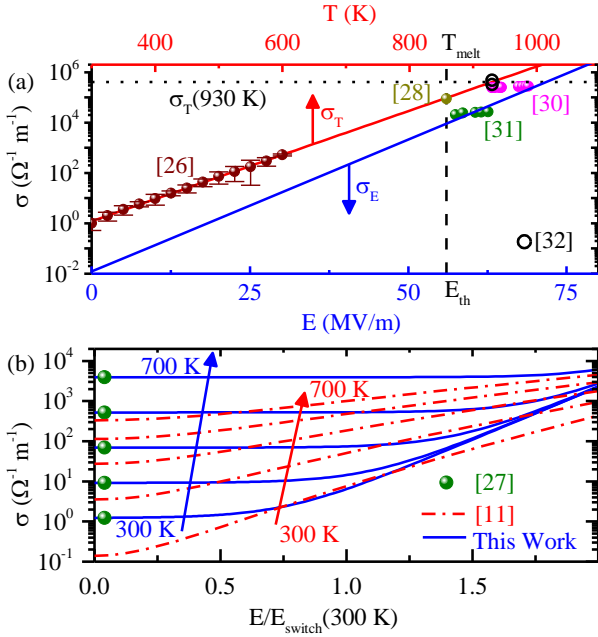


Fig. 3: (a) T and \vec{E} dependent contributions to electrical conductivity in (1); temperature is uncertain for $T > T_{melt}$. (b) Conductivity-Field behavior using the model in this work (metastable a-GST) and the model in [19] (drifted, doped a-GST) at various temperatures. We use $E_{switch}(300\text{ K}) = 25.01\text{ MV/m}$ in this work and $E_{switch}(300\text{ K}) = 155\text{ MV/m}$ for the curves in [19].

a band edge via independent thermal and electrical processes:

$$\sigma_a(T, \vec{E}) = \min(q(n_T + n_E)\mu, \sigma_{max}), \quad (2)$$

where n_T and n_E are carriers excited via thermal or electrical processes and μ is the free carrier mobility.

We fit σ_T to low- \vec{E} measurements of metastable a-GST wires [27] and molten GST thin films [28], as described in [29] (Fig. 3a). Measurements of liquid GST show a semiconductor-to-metal transition near 930 K [30], with σ becoming practically independent of T . We therefore limit $\sigma_a(T, \vec{E})$ to $\sigma_T(930\text{ K}) = 4.1 \times 10^5\text{ }[\Omega^{-1}\text{ m}^{-1}]$, which is in line with the highest conductivities measured in molten GST [30]–[32] (Fig. 3a).

σ_E is assumed to be an exponential which contributes 1% of $\sigma_T(300\text{ K})$ at zero field and 10% of $\sigma_T(T_{melt})$ at E_{th} :

$$\sigma_E(\vec{E}) = \frac{\sigma_T(300\text{ K})}{100} \exp(|\vec{E}| \cdot C_1) \quad (3)$$

where $C_1 = 2.42 \times 10^{-7}\text{ m/V}$ is chosen such that $\sigma_E(E_{th}) = \sigma_T(T_{melt}) \times 10\%$. We use $E_{th} = 56\text{ MV/m}$, the breakdown field measured in as-deposited a-GST [33], and $T_{melt} = 858\text{ K}$ [28] (Fig. 3a).

We include σ - \vec{E} curves at various temperatures calculated using the models in this work (for metastable a-GST) and the models in [19] (for drifted, doped a-GST) for comparison (Fig. 3b). σ_T dominates at low fields, while σ_E begins to dominate at higher and higher fields with increasing T .

We couple heat transfer and current continuity physics to simulate transient device operation, including temperature

dependent thermoelectric effects [34]:

$$d_m c_p \frac{dT}{dt} - \nabla \cdot (k \nabla T) = -\nabla V \cdot J - \nabla \cdot (J S T) + q_H \quad (4)$$

$$\nabla \cdot J = \nabla \cdot (-\sigma \nabla V - \sigma S \nabla T) = 0 \quad (5)$$

where d_m is mass density, c_p is specific heat, t is time, k is thermal conductivity, V is electric potential, J is current density, S is the Seebeck coefficient, and q_H accounts for the latent heat of phase change. We use temperature dependent parameters for a-GST, crystalline GST (c-GST), TiN, and SiO_2 as in [23], [25].

We model phase change as

$$\frac{d\vec{CD}}{dt} = \overrightarrow{Nucleation} + \overrightarrow{Growth} + \overrightarrow{Melt}, \quad (6)$$

where \vec{CD} is a 2-vector whose magnitude (CD) corresponds to phase ($CD = 0$ or 1 for the amorphous or crystalline phase) and whose orientation (θ_{CD}) corresponds to grain orientation ($\tan(\theta_{CD}) = CD_2/CD_1$), capturing nucleation, growth, and grain boundary melting [23], [25]. We solve for (6) in PCM devices but not OTS devices, which we assume do not crystallize in our simulations.

III. SIMULATIONS

We first simulate switching in 3D and 2D-rotational geometries by applying a $3\text{V}/60\text{ ns}$ triangular pulse (Fig. 2a,b). Results show filamentary switching with current confined to the central portion of the device (Fig. 4a-j), with practically identical I - V characteristics for 3D and 2D-rotational simulations (Fig. 2c). 3D simulations show some instability of the filament location (slightly off-center in Fig. 4d,i) and filament migration over time.

We next evaluate the impact of σ_E by simulating switching with $\sigma_E = 0$ (Fig. 5a) and compare the results with σ_E defined as in (3) (Fig. 5b). V_{switch} and I_{switch} are the values at which V_{Device} begins to decrease. Threshold switching occurs even with $\sigma_E = 0$ due to thermal runaway. However, defining σ_E as in (3) gives a switching field ($E_{switch} = V_{switch} / h_{OTS}$) that is smaller and less dependent on h_{OTS} (Fig. 5c). Some h_{OTS} dependence is still observed due to changing thermal conditions.

Reference [33] reports switching fields from 8.1 MV/m (as-deposited a- $\text{Ge}_{15}\text{Sb}_{85}$) to 94 MV/m (as-deposited 4 nm thick a-Sb). We examine the tunability of our model by varying E_{th} in (3) from 5.6 to 560 MV/m (Fig. 6). Results show E_{switch} varying from 5 to 42.5 MV/m . $E_{switch} = 25.01\text{ MV/m}$ when $E_{th} = 56\text{ MV/m}$, similar to the $E_{switch} = 28.75\text{ MV/m}$ measured in [13] for melt-quenched a-GST. σ_E becomes negligible compared to σ_T when $E_{th} > 200\text{ MV/m}$ even for high fields: the σ_T used in this work precludes $E_{switch} > 42.5\text{ MV/m}$; a reduced σ_T is required for higher switching fields. I_{switch} decreases by $\sim 100\times$ as V_{switch} increases, resulting in a decrease in switching power (P_{switch}) from ~ 100 to $20\text{ } \mu\text{W}$ (Fig. 6c).

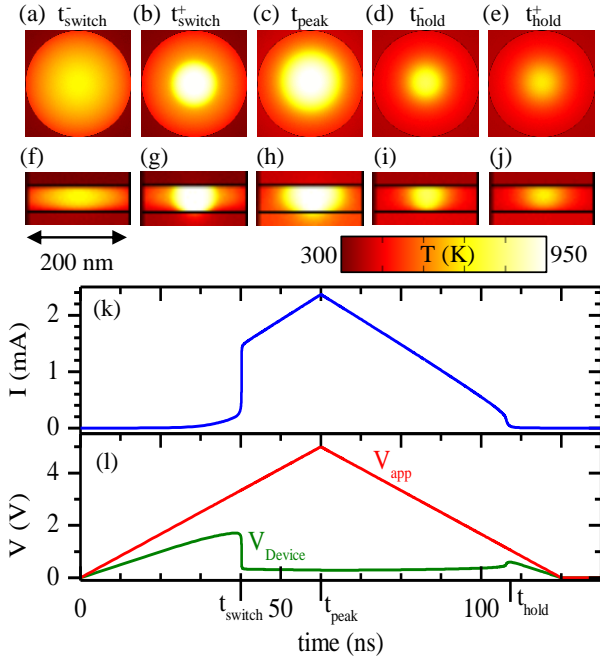


Fig. 4: (a-e) x-y and (f-j) x-z temperature cut planes while switching the 3D OTS in Fig. 2a illustrate filamentary on-state conduction. (j) Current and (k) device voltage transients resulting from the applied V_{app} used to generate the I-V in Fig. 2c. Superscripts “-” and “+” refer to the time steps (1 ns increments) before and after the subscripted event. (Fig. 2a: $R_{\text{Load}} = 1 \text{ k}\Omega$, $h_{\text{OTS}} = 50 \text{ nm}$, $r_{\text{OTS}} = 100 \text{ nm}$, $V_{\text{app}} = 5 \text{ V} / 60 \text{ ns}$ triangular pulse).

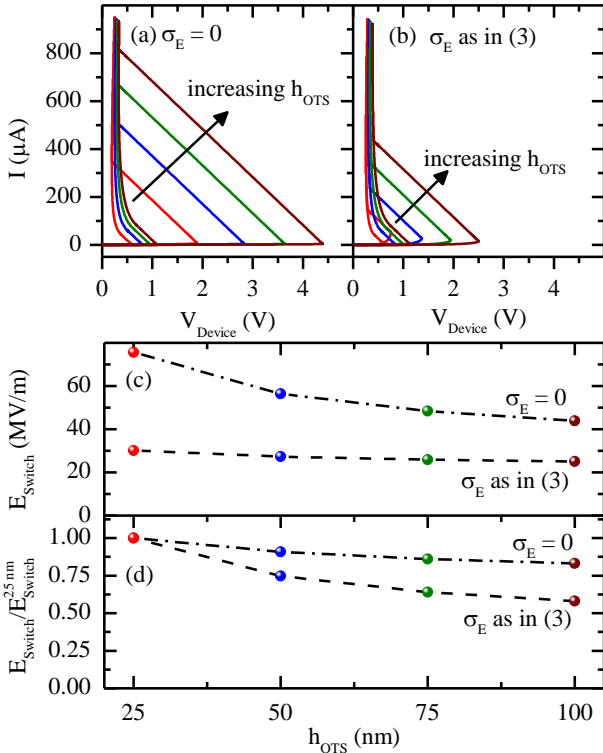


Fig. 5: The switching voltage increases with h_{OTS} both (a) without and (b) with field dependent conductivity. Including field dependent conductivity reduces the switching field’s (c) magnitude and (d) sensitivity to h_{OTS} . (Fig. 2b: $R_{\text{Load}} = 5 \text{ k}\Omega$, $h_{\text{OTS}} = 25$ to 100 nm , $r_{\text{OTS}} = 100 \text{ nm}$, $V_{\text{app}} = 5 \text{ V} / 5 \text{ ns}$ triangular pulse).

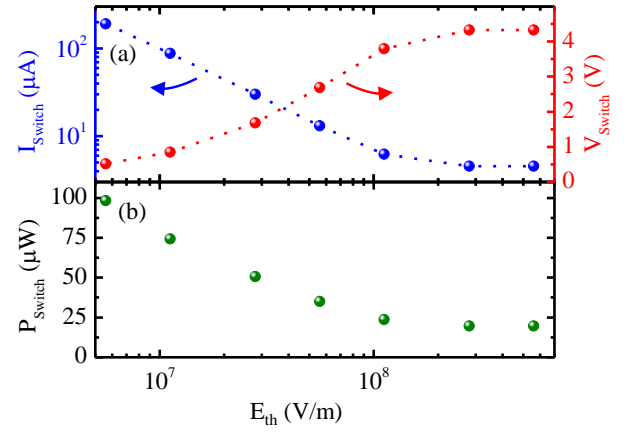


Fig. 6: (a) The switching current (voltage) decreases (increases) and (c) the switching power decreases with increasing E_{th} in (3). The device switches thermally before the field contribution becomes significant for $E_{\text{th}} > 1 \times 10^8 \text{ V/m}$. As a result, further increases to E_{th} result in the same switching characteristics. (Fig. 2b: $R_{\text{Load}} = 5 \text{ k}\Omega$, $h_{\text{OTS}} = 100 \text{ nm}$, $r_{\text{OTS}} = 100 \text{ nm}$, $V_{\text{app}} = 5 \text{ V} / 5 \text{ ns}$ triangular pulse).

V_{Switch} has been shown to decrease with increasing ambient temperature (T_{ambient}), while the temperature behavior of I_{Switch} and P_{Switch} are less clear [19]. We simulate switching while varying T_{ambient} (the initial temperature and the fixed top and bottom TiN boundary temperatures, Fig. 2b) from 300 to 400 K (Fig. 7). V_{Switch} decreases as expected (Fig. 7a). I_{Switch} at first decreases and then increases with increasing T_{ambient} , while P_{Switch} monotonously decreases in the T_{ambient} range simulated but is beginning to flatten with increasing T by 400 K.

Next, we systematically vary r_{OTS} , h_{OTS} , and the rise time (τ_{rise}) of V_{app} in the geometry shown in Fig. 2b (Fig. 8). Results agree with expected OTS behavior: V_{Switch} approximately doubles as h_{OTS} doubles [6], V_{Switch} decreases with increasing τ_{rise} , approaching a minimum value [16], I_{hold} and V_{hold} are only weakly dependent on h_{OTS} [15], and switching characteristics are only weakly dependent on r_{OTS} due to filamentary conduction in the on-state.

Finally, we simulate an OTS and PCM in series (OTS+PCM, Fig. 1) based on the devices fabricated and characterized in [1]. We use a 2D, 45 nm fixed out-of-plane-depth simulation instead of a 2D-rotational simulation to more appropriately model phase change dynamics in the PCM with (6). We use a 500 nm depth in the bit line to account for its large thermal mass (Fig. 1), set $T_{\text{ambient}} = 300 \text{ K}$ as the initial and fixed TiN boundary temperatures, and reset the device with a 5 V / 5 ns square pulse (1 ns rise and fall times) at V_{app} followed by 1 μs for thermalization (starting at Fig. 1 and ending at Fig. 9a). We then sweep V_{app} from 0 to 2.5 V over 50 ns to characterize the OTS + reset PCM. We also simulate an isolated OTS and isolated reset PCM in the same way by replacing the PCM or OTS, respectively, with TiN (Fig. 9c,d). We plot the I - V characteristics before switching, dividing currents and voltages by the isolated OTS I_{Switch} and V_{Switch} values in order to compare

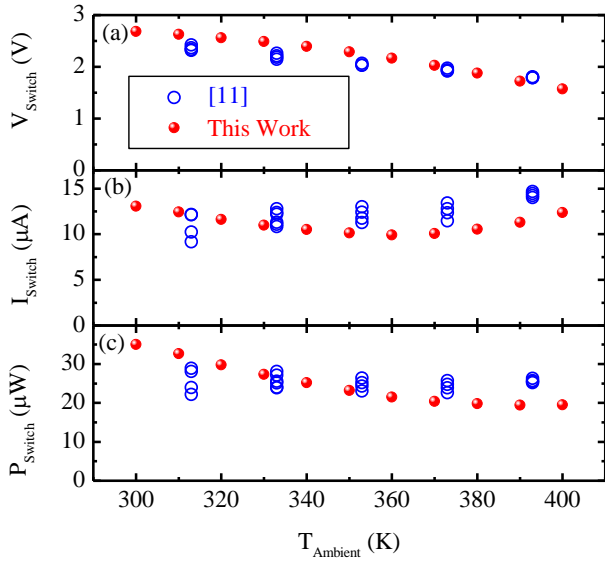


Fig. 7: The (a) voltage, (b) current, and (c) power required to switch as the ambient temperature changes. V_{switch} decreases monotonically, but I_{switch} and P_{switch} have more complex relationships with $T_{ambient}$. (Fig. 2b: $R_{Load} = 5 \text{ k}\Omega$, $h_{OTS} = r_{OTS} = 100 \text{ nm}$, $V_{app} = 5 \text{ V} / 5 \text{ s}$ triangular pulse).

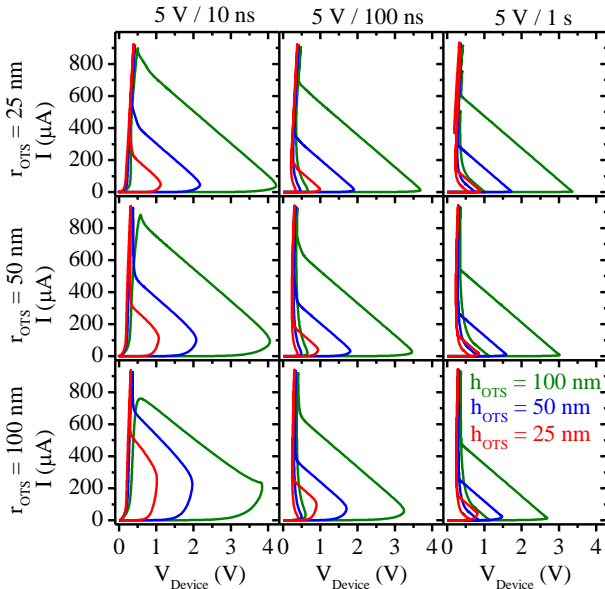


Fig. 8: Switching characteristics of OTS devices with varying radii, ramp times, and heights. The simulated holding currents and voltages are weakly dependent on h_{OTS} , but the switching voltage \sim doubles as h_{OTS} doubles. (Geometry in Fig. 2b).

our results to those presented in [1] (Fig. 9e). The results are similar, with the OTS limiting the current in the reset PCM until $V_{Device} / V_{switch}^{OTS} > 2$ (Fig. 9d). This limits the current during read in a reset cell while allowing high current in a set cell, creating a large read margin. The smaller scaled currents for the PCM and OTS+PCM in our simulation could be due to a difference in the amorphous volume in the reset PCM; the fixed out-of-plane depth in our simulations, which cannot capture filaments smaller than 45 nm in depth and may thus overestimate I_{switch} in the OTS; or parameter differences

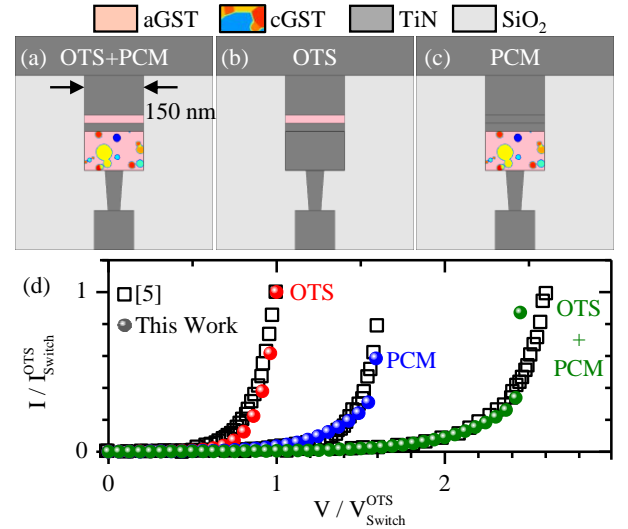


Fig. 9: (a) Reset OTS+PCM, (b) isolated OTS, and (c) isolated reset PCM. (d) Pre-switching I-V characteristics scaled by V_{switch} and I_{switch} in the OTS using the model in this work (spheres) and experimental data extracted from [1] (squares). I-V characteristics from this work show similar switching voltages but lower scaled switching currents. The schematic of the simulation setup is shown in Fig. 1. The OTS+PCM reset animation for this simulation is available in supplementary material.

between aGST and the (unreported) OTS material used in [1].

IV. CONCLUSION

The coupling of thermal and electric field contributions to electrical conductivity in amorphous semiconductors is complex, as evidenced by the large number of physical models proposed to explain the same characteristics. Our modeling results show that threshold switching and ‘snap-back’ observed in OTS and PCM devices can be explained through electro-thermal phenomena giving rise to thermal run-away and filamentary conduction and can be modeled efficiently with a finite element framework.

V. ACKNOWLEDGEMENTS

The authors would like to thank Ilya Karpov of Intel Corporation, Martin Salinga of RWTH Aachen University, Abu Sebastian of IBM Zurich, and Geoffrey Burr of IBM Almaden for valuable discussions.

REFERENCES

- [1] D. Kau, S. Tang, I. V. Karpov, R. Dodge, B. Klehn, J. A. Kalb, J. Strand, A. Diaz, N. Leung, J. Wu, S. Lee, T. Langtry, K. W. Chang, C. Papagianni, J. Lee, J. Hirst, S. Erra, E. Flores, N. Righos, *et al.*, “A stackable cross point phase change memory,” in *Technical Digest - International Electron Devices Meeting, IEDM*, 2009, pp. 1–4 DOI:10.1109/IEDM.2009.5424263.
- [2] F. Xia, J. Xiong, and N.-H. Sun, “A Survey of Phase Change Memory Systems,” *J. Comput. Sci. Technol.*, vol. 30, no. 1, pp. 121–144, 2015 DOI:10.1007/s11390-015-1509-2.
- [3] H.-S. P. Wong, S. Raoux, S. Kim, J. Liang, J. P. Reifenberg, B. Rajendran, M. Asheghi, and K. E. Goodson, “Phase Change Memory,” *Proc. IEEE*, vol. 98, no. 12, pp. 2201–2227, 2010

- DOI:10.1109/JPROC.2010.2070050.
- [4] A. Chen, *Memory Selector Devices and Crossbar Array Design: A Modeling Based Assessment*, vol. 16, no. 4, Springer US, 2017, pp. 1186–1200 DOI:10.1016/j.cub.2015.10.018.
- [5] G. W. Burr, R. S. Shenoy, K. Virwani, P. Narayanan, A. Padilla, B. Kurdi, and H. Hwang, “Access devices for 3D crosspoint memory,” *J. Vac. Sci. Technol. B, Nanotechnol. Microelectron. Mater. Process. Meas. Phenom.*, vol. 32, no. 4, p. 040802, 2014 DOI:10.1116/1.4889999.
- [6] S. R. Ovshinsky, “Reversible electrical switching phenomena in disordered structures,” *Phys. Rev. Lett.*, vol. 21, no. 20, pp. 1450–1453, Nov. 1968 DOI:10.1103/PhysRevLett.21.1450.
- [7] T. Matsunaga, J. Akola, S. Kohara, T. Honma, K. Kobayashi, E. Ikenaga, R. O. Jones, N. Yamada, M. Takata, and R. Kojima, “From local structure to nanosecond recrystallization dynamics in AgInSbTe phase-change materials,” *Nat. Mater.*, vol. 10, no. 2, pp. 129–134, 2011 DOI:10.1038/nmat2931.
- [8] M. Anbarasu, M. Wimmer, G. Bruns, M. Salinga, and M. Wuttig, “Nanosecond threshold switching of GeTe 6 cells and their potential as selector devices,” *Appl. Phys. Lett.*, vol. 100, no. 14, 2012 DOI:10.1063/1.3700743.
- [9] M. J. Lee, D. Lee, H. Kim, H. S. Choi, J. B. Park, H. G. Kim, Y. K. Cha, U. I. Chung, I. K. Yoo, and K. Kim, “Highly-scalable threshold switching select device based on chalcogenide glasses for 3D nanoscaled memory arrays,” *Tech. Dig. - Int. Electron Devices Meet. IEDM*, no. December, pp. 10–13, 2012 DOI:10.1109/IEDM.2012.6478966.
- [10] J. Choe, “Intel 3D XPoint Memory Die Removed from Intel Optane™ PCM (Phase Change Memory),” *Tech Insights*, 2017. [Online]. Available: <https://www.techinsights.com/about-techinsights/overview/blog/intel-3d-xpoint-memory-die-removed-from-intel-optane-pcm/>. [Accessed: 10-Dec-2018].
- [11] R. W. Pryor and H. K. Henisch, “Nature of the on-state in chalcogenide glass threshold switches,” *J. Non. Cryst. Solids*, vol. 7, no. 2, pp. 181–191, 1972 DOI:10.1016/0022-3093(72)90288-8.
- [12] K. E. Petersen, “On state of amorphous threshold switches,” *J. Appl. Phys.*, vol. 47, no. 1976, p. 256, 1976 DOI:10.1063/1.322309.
- [13] D. Ielmini, “Threshold switching mechanism by high-field energy gain in the hopping transport of chalcogenide glasses,” *Phys. Rev. B - Condens. Matter Mater. Phys.*, vol. 78, no. 3, pp. 1–8, Jul. 2008 DOI:10.1103/PhysRevB.78.035308.
- [14] M. Nardone, V. G. Karpov, D. C. S. S. Jackson, and I. V. Karpov, “A unified model of nucleation switching,” *Appl. Phys. Lett.*, vol. 94, no. 10, pp. 10–12, Mar. 2009 DOI:10.1063/1.3100779.
- [15] W. Czubatjy and S. J. Hudgens, “Invited paper: Thin-film Ovonic threshold switch: Its operation and application in modern integrated circuits,” *Electron. Mater. Lett.*, vol. 8, no. 2, pp. 157–167, 2012 DOI:10.1007/s13391-012-2040-z.
- [16] M. Wimmer and M. Salinga, “The gradual nature of threshold switching,” *New J. Phys.*, vol. 16, 2014 DOI:10.1088/1367-2630/16/11/113044.
- [17] A. Athmanathan, D. Krebs, A. Sebastian, M. Le Gallo, H. Pozidis, and E. Eleftheriou, “A finite-element thermoelectric model for phase-change memory devices,” *Int. Conf. Simul. Semicond. Process. Devices, SISPAD*, vol. 2015–Octob, pp. 289–292, 2015 DOI:10.1109/SISPAD.2015.7292316.
- [18] M. Le Gallo, M. Kaes, A. Sebastian, and D. Krebs, “Subthreshold electrical transport in amorphous phase-change materials,” *New J. Phys.*, vol. 17, no. 9, 2015 DOI:10.1088/1367-2630/17/9/093035.
- [19] M. Le Gallo, A. Athmanathan, D. Krebs, and A. Sebastian, “Evidence for thermally assisted threshold switching behavior in nanoscale phase-change memory cells,” *J. Appl. Phys.*, vol. 119, no. 2, 2016 DOI:10.1063/1.4938532.
- [20] M. Nardone, M. Simon, I. V. Karpov, and V. G. Karpov, “Electrical conduction in chalcogenide glasses of phase change memory,” *J. Appl. Phys.*, vol. 112, no. 7, 2012 DOI:10.1063/1.4738746.
- [21] I. V. Karpov, M. Mitra, D. Kau, G. Spadini, Y. A. Kryukov, and V. G. Karpov, “Evidence of field induced nucleation in phase change memory,” *Appl. Phys. Lett.*, vol. 92, no. 17, pp. 4–6, 2008 DOI:10.1063/1.2917583.
- [22] Z. Woods and A. Gokirmak, “Modeling of Phase-Change Memory: Nucleation, Growth, and Amorphization Dynamics During Set and Reset: Part I—Effective Media Approximation,” *IEEE Trans. Electron Devices*, vol. 64, no. 11, pp. 4466–4471, Nov. 2017 DOI:10.1109/TED.2017.2745506.
- [23] Z. Woods, J. Scoggin, A. Cywar, L. Adnane, and A. Gokirmak, “Modeling of Phase-Change Memory: Nucleation, Growth, and Amorphization Dynamics during Set and Reset: Part II - Discrete Grains,” *IEEE Trans. Electron Devices*, vol. 64, no. 11, pp. 4472–4478, Nov. 2017 DOI:10.1109/TED.2017.2745500.
- [24] J. Scoggin, R. S. Khan, H. Silva, and A. Gokirmak, “Modeling and impacts of the latent heat of phase change and specific heat for phase change materials,” *Appl. Phys. Lett.*, vol. 112, no. 19, p. 193502, 2018 DOI:10.1063/1.5025331.
- [25] J. Scoggin, Z. Woods, H. Silva, and A. Gokirmak, “Modeling heterogeneous melting in phase change memory devices,” *Appl. Phys. Lett.*, vol. 114, no. 4, pp. 1–6, Oct. 2019 DOI:10.1063/1.5067397.
- [26] A. Faraclas, N. Williams, A. Gokirmak, and H. Silva, “Modeling of set and reset operations of phase-change memory cells,” *IEEE Electron Device Lett.*, vol. 32, no. 12, pp. 1737–1739, Dec. 2011 DOI:10.1109/LED.2011.2168374.
- [27] F. Dirisaglik, G. Bakan, Z. Jurado, S. Muneer, M. Akbulut, J. Rarey, L. Sullivan, M. Wennberg, A. King, L. Zhang, R. Nowak, C. Lam, H. Silva, A. Gokirmak, and others, “High speed, high temperature electrical characterization of phase change materials: metastable phases, crystallization dynamics, and resistance drift,” *Nanoscale*, vol. 7, no. 40, pp. 16625–16630, Oct. 2015 DOI:10.1039/C5NR0512A.
- [28] L. Adnane, N. Williams, H. Silva, and A. Gokirmak, “High temperature setup for measurements of Seebeck coefficient and electrical resistivity of thin films using inductive heating,” *Rev. Sci. Instrum.*, vol. 86, no. 10, p. 105119, Oct. 2015 DOI:10.1063/1.4934577.
- [29] S. Muneer, J. Scoggin, F. Dirisaglik, L. Adnane, A. Cywar, G. Bakan, K. Cil, C. Lam, H. Silva, and A. Gokirmak, “Activation energy of metastable amorphous Ge₂Sb₂Te₅ from room temperature to melt,” *AIP Adv.*, vol. 8, no. 6, p. 065314, 2018 DOI:10.1063/1.5035085.
- [30] R. Endo, S. Maeda, Y. Jinnai, R. Lan, M. Kuwahara, Y. Kobayashi, and M. Susa, “Electric resistivity measurements of Sb₂Te₃ and Ge₂Sb₂Te₅ melts using four-terminal method,” *Jpn. J. Appl. Phys.*, vol. 49, no. 6, p. 5802, 2010 DOI:10.1143/JJAP.49.065802.
- [31] T. Kato and K. Tanaka, “Electronic Properties of Amorphous and Crystalline Ge₂Sb₂Te₅ Films,” *Jpn. J. Appl. Phys.*, vol. 44, no. 10, pp. 7340–7344, 2005 DOI:10.1143/JJAP.44.7340.
- [32] K. Cil, F. Dirisaglik, and L. Adnane, “Electrical resistivity of liquid based on thin-film and nanoscale device measurements,” *on Electron Devices*, 2013.
- [33] D. Krebs, S. Raoux, C. T. Rettner, G. W. Burr, M. Salinga, and M. Wuttig, “Threshold field of phase change memory materials measured using phase change bridge devices,” *Appl. Phys. Lett.*, vol. 95, no. 8, pp. 1–4, 2009 DOI:10.1063/1.3210792.
- [34] G. Bakan, N. Khan, H. Silva, and A. Gokirmak, “High-temperature thermoelectric transport at small scales: Thermal generation, transport and recombination of minority carriers,” *Sci. Rep.*, vol. 3, no. 1, p. 2724, 2013 DOI:10.1038/srep02724.



Jake Scoggin received his B.S. degree in Nanosystems Engineering from Louisiana Tech University in 2012 and his M.S. degree in Electrical Engineering from Louisiana Tech University in 2014. He is a PhD student in Electrical & Computer Engineering at the University of Connecticut since 2014.



Helena Silva received her B.S. degree in Engineering Physics from the University of Lisbon, Portugal in 1998 and her M.S. and Ph.D. degrees in Applied Physics from Cornell University in 2002 and 2005. She is currently an Associate Professor of Electrical and Computer Engineering at the University of Connecticut. Her research focuses on electronics devices for logic, memory, and energy conversion.



Ali Gokirmak received his B.S. degrees in Electrical Engineering and Physics from University of Maryland at College Park in 1998 and received his Ph.D. in Electrical and Computer Engineering from Cornell University in 2005. He joined the Electrical & Computer Engineering Department of the University of Connecticut in 2006, where he is currently an associate professor .